Thermal loads and trajectory simulation analysis of space shuttle re-entry hypersonic flights

E. E. Panagiotopoulos, D. P. Margaris and D. G. Papanikas
Fluid Mechanics Laboratory, Mechanical Engineering and Aeronautics Department,
University of Patras, GR-26500, Patras, Greece

Abstract

A full-synthesized aerothermodynamics trajectory simulation analysis is developed for the atmospheric hypersonic re-entry flight missions. An analytical method is applied for hypervelocity aerodynamic coefficients, based on modified Newtonian Flow model. Real gas effects are taken into account by means of the thermodynamic and transport properties of equilibrium air in high entry temperatures. Convective stagnation heating loads are being calculated using a new engineering correlation, based on suitable modifications of the full classical Fay-Riddell theory. The efficiency of the present method is proven by comparisons with published data of verified experiments and computational codes on Space Shuttle flight analysis.

1. Introduction

The prediction of aerodynamic heating in design of most re-entry spacecrafts (S/C) into the Earth's atmosphere is essential for a successful space mission and a safe return. Various methods of aero-thermodynamic analysis have been based on a combination of theoretical and numerical techniques in order to find accurately characteristic magnitudes of the critical stagnation region such as wall temperature and heat transfer distributions for re-entry space vehicles[1,2]. Recent experimental investigations have provided further data of the complicated heating environment[3,4].

After the STS-107 Columbia[5] disintegrated over Texas on its return flight to Earth, a full-synthesized aerothermodynamics trajectory simulation is developed for the hypersonic re-entry flight missions of Space Shuttle vehicles. The aerothermodynamic analysis for entry flight takes into consideration the real gas effects and a new engineering correlation convective-heating method is proposed about blunt re-entry ballistic and lifting spacecrafts for equilibrium air as a chemically reacting gas mixture for constant entropy edge conditions. Also an analytical engineering technique is applied for the estimation of the aerodynamic coefficients during the critical hypersonic flight regime, based on the modified Newtonian Flow theory. The efficiency of the above synthetic coupled method is proven by comparisons with computational and experimental data of known entry Space Shuttle flight missions.

2. Trajectory flight path model

A three-degree-of-freedom rigid-spacecraft point mass model[1,6] is employed to predict the dynamics of an atmospheric entry/reentry flight path trajectory. It comprises the three translational components (radial position r, longitude θ, latitude φ) describing the S/C's position and the three force components (velocity V, flight path angle γ, heading angle ψ) for the orientation of S/C's motion with respect to Figure 1:

The standard kinematic expression and the Newton's second law are applied for the present physicomathematical model, with respect to the body-rotating coordinate system Oxyz, as:

$$\vec{V} = \frac{d\vec{r}}{dt} = \dot{\vec{r}} \qquad m\frac{d\vec{V}}{dt} = \vec{F}_{tot} - \vec{a}_{Cor} - \vec{a}_{Centr} \qquad \textbf{(1, 2)}$$

The total S/C's velocity vector and the time derivative of the radial distance from the planet's center can be expressed in the rotating reference frame as:

$$\dot{\vec{r}} = \begin{Bmatrix} \dot{r}_X \\ \dot{r}_Y \\ \dot{r}_Z \end{Bmatrix} = \begin{bmatrix} 1 & 0 & 0 \\ 0 & rc_\varphi & 0 \\ 0 & 0 & r \end{bmatrix} \begin{Bmatrix} \dot{r} \\ \dot{\vartheta} \\ \dot{\varphi} \end{Bmatrix} \qquad \vec{V} = \begin{Bmatrix} V_X \\ V_Y \\ V_Z \end{Bmatrix} = \begin{Bmatrix} \dot{r}_X \\ \dot{r}_Y \\ \dot{r}_Z \end{Bmatrix} = V \begin{Bmatrix} s_\gamma \\ c_\gamma c_\psi \\ c_\gamma s_\psi \end{Bmatrix} \qquad \textbf{(3, 4)}$$

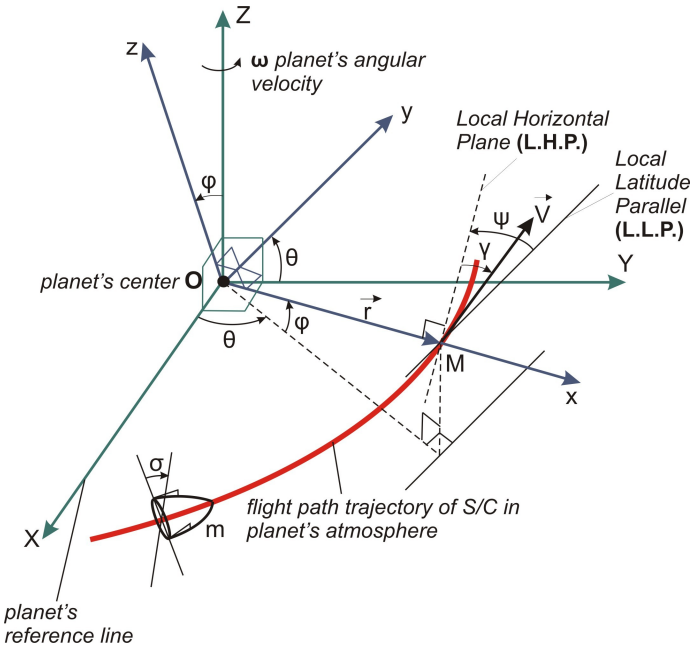

Figure 1: Coordinate systems for the entry flight motion of a space vehicle in a planetary atmosphere.

Comparing the two Eqs (3, 4) with Eq. (1), three first order ordinary differential expressions are derived:

$$\dot{r} = Vs_\gamma \qquad \dot{\vartheta} = \frac{Vc_\gamma c_\psi}{rc_\varphi} \qquad \dot{\varphi} = \frac{Vc_\gamma s_\psi}{r} \qquad \textbf{(5, 6, 7)}$$

The Coriolis and centrifugal accelerations in Eq. (2), due to the constant angular motion ω of the planet, are expressed in the rotating reference frame Oxyz as:

$$\vec{a}_{Cor}=\begin{Bmatrix}a_{CorX}\\a_{CorY}\\a_{CorZ}\end{Bmatrix}=2\omega V\begin{Bmatrix}-c_\gamma c_\varphi c_\psi\\-c_\gamma s_\varphi s_\psi+s_\gamma c_\varphi\\c_\gamma s_\varphi c_\psi\end{Bmatrix}\qquad \vec{a}_{Centr}=\begin{Bmatrix}a_{CentrX}\\a_{CentrY}\\a_{CentrZ}\end{Bmatrix}=\omega^2 r\begin{Bmatrix}-c_\varphi^2\\0\\s_\varphi c_\varphi\end{Bmatrix} \quad \textbf{(8, 9)}$$

The total force F_{tot} acting on S/C's vehicle comprises the weight (gravitational) force F_{weight}, the aerodynamic force F_A, which can be decomposed into a drag force F_D opposite to the velocity vector V and a lift force F_L perpendicular to V, and the thrust force vector F_T. The combination of forces gives

$$\vec{F}_{tot}=\begin{Bmatrix}X_{tot}\\Y_{tot}\\Z_{tot}\end{Bmatrix}=\begin{Bmatrix}X_{weight}\\Y_{weight}\\Z_{weight}\end{Bmatrix}+\begin{Bmatrix}X_{At}\\Y_{At}\\Z_{At}\end{Bmatrix}+\begin{Bmatrix}X_{An}\\Y_{An}\\Z_{An}\end{Bmatrix} \quad \textbf{(10)}$$

The weight force and the total aerodynamic force vectors F_{At} and F_{An} (tangential and normal to the flight path trajectory, respectively) are considered acting on the S/C's center of gravity. They can be expressed in the forms:

$$\vec{F}_{weight}=\begin{Bmatrix}X_{weight}\\Y_{weight}\\Z_{weight}\end{Bmatrix}=mg\begin{Bmatrix}-1\\0\\0\end{Bmatrix}\qquad \vec{F}_{At}=\begin{Bmatrix}X_{At}\\Y_{At}\\Z_{At}\end{Bmatrix}=F_{tang.}\begin{Bmatrix}s_\gamma\\c_\gamma c_\psi\\c_\gamma s_\psi\end{Bmatrix} \quad \textbf{(11, 12)}$$

$$\vec{F}_{An}=\begin{Bmatrix}X_{An}\\Y_{An}\\Z_{An}\end{Bmatrix}=F_{norm.}\begin{Bmatrix}c_\sigma c_\gamma\\-c_\sigma s_\gamma c_\psi-s_\sigma s_\psi\\-c_\sigma s_\gamma s_\psi+s_\sigma c_\psi\end{Bmatrix} \quad \textbf{(13)}$$

where $F_{tang.}=F_T c_\varepsilon-F_D=F_T c_\varepsilon-0.5C_D\rho V^2 S_{ref}$ and $F_{norm.}=F_T s_\varepsilon+F_L=F_T s_\varepsilon+0.5C_L\rho V^2 S_{ref}$.

The total acceleration of the vehicle can be expressed in the rotating coordinate system's axes with the formula:

$$\frac{d\vec{V}}{dt}=\begin{Bmatrix}\dot V_X\\\dot V_Y\\\dot V_Z\end{Bmatrix}=\begin{bmatrix}s_\gamma & Vc_\gamma & 0\\c_\gamma c_\psi & -Vs_\gamma c_\psi & -Vc_\gamma s_\psi\\c_\gamma s_\psi & -Vs_\gamma s_\psi & Vc_\gamma c_\psi\end{bmatrix}\begin{Bmatrix}\dot V\\\dot\gamma\\\dot\psi\end{Bmatrix}+\frac{V^2}{r}c_\gamma\begin{Bmatrix}-c_\gamma\\c_\psi\left(s_\gamma-c_\gamma s_\psi t_\varphi\right)\\s_\gamma s_\psi+c_\gamma c_\psi^2 t_\varphi\end{Bmatrix} \quad \textbf{(14)}$$

Comparing the two Eqs (2, 14) in addition to Eqs (8-9, 10-13) for the total S/C's acceleration dV/dt, three linear equations are derived with the three unknown variables of velocity V, flight path angle γ and heading angle ψ. Solving this equation system and emitting intermediate manipulations, the following set of equations is derived:

$$\dot V=\frac{F_{tang.}}{m}-gs_\gamma+\omega^2 r c_\varphi\left(s_\gamma c_\varphi-c_\gamma s_\varphi s_\psi\right) \quad \textbf{(15)}$$

$$\dot{\gamma} = \frac{F_{norm}}{mV} c_\sigma + \left(\frac{V}{r} - \frac{g}{V} \right) c_\gamma + 2\omega c_\varphi c_\psi + \frac{\omega^2 r}{V} c_\varphi \left(c_\gamma c_\varphi + s_\gamma s_\varphi s_\psi \right) \quad \textbf{(16)}$$

$$\dot{\psi} = \frac{F_{norm}}{mV} \frac{s_\sigma}{c_\gamma} - \frac{V}{r} c_\gamma c_\psi t_\varphi + 2\omega \left(t_\gamma c_\varphi s_\psi - s_\varphi \right) - \frac{\omega^2 r}{V c_\gamma} s_\varphi c_\varphi c_\psi \quad \textbf{(17)}$$

During the entire atmospheric flight is applied a method of navigation by appropriate pre-determined suitable maneuvering variations of bank angle σ and angle of attack α, in order to maintain low levels of deceleration and heating transfer rates, especially for the manned STS space vehicles. The coefficients C_L, C_D are spacecraft-specific functions of the atmospheric Mach number flight motion and angle of attack variations.

The dynamic expressions of motion in Eqs (5-7, 15-17) are highly nonlinear. Thus, numerical integration using a 4th order Runge-Kutta method is commonly used to obtain solutions to this initial value problem of the 3-D S/C's atmospheric flight. Due to the fact that aerodynamic data only in the hypersonic regime are available, we define a final Mach number condition $M_f = 3$.

The free-stream temperature, density and pressure properties are calculated as a function of altitude from the U.S. Standard Atmosphere 1976 atmospheric model. A gravitational acceleration model $g(r,\varphi)$ is applied[6], which expands into spherical harmonics of up to 5th order as a function of the position vector $\vec{r}$ and latitude φ.

2.1 Space shuttle aerodynamic model

In order to determine the aerodynamic coefficients of the Space Shuttle in the hypersonic regime, a modified Finite Wing Span Newtonian Flow model[7] is applied. The simplicity of this method only needs the spacecraft's geometry taking into account finite and non-constant wing span in conjunction with a small number of experimental data.

Wing surface can be modelled with various ways like straight lines, polynomial or exponential curves, etc. In the present analysis the wing's top view surface is considered to be flat and a simplified five straight-line technique is applied between known and properly predetermined points.

As shown in Figure 2, the coordinates of the five points are $(x_1, y_1) = (0, 0)$, $(x_2, y_2) = (19.672, 4.64)$, $(x_3, y_3) = (26.256, 11.2)$, $(x_4, y_4) = (31.179, 11.2)$ and $(x_5, y_5) = (32.82, 0)$, respectively. The corresponding mathematical equations of lines between these points are expressed in the following forms: $y_a = y_1 = 0.236x$, $y_b = y_2 = 0.9963x - 14.96$, $y_c = y_3 = 11.2$, $y_d = y_4 = -6.8251x + 224.0$.

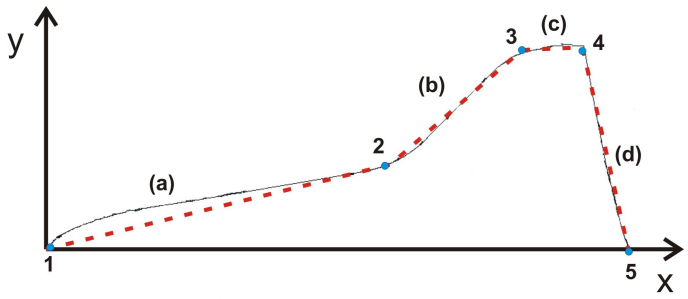

Figure 2: Space Shuttle Orbiter half wing surface geometry modelled with straight lines.

The total normal force coefficient C_N acting on the S/C's center of gravity is estimated from the known expression:

$$C_N = 2\frac{1}{S_{ref}} \int_0^c \left(C_{p,l} - C_{p,u} \right) y dx \;\rightarrow\; C_N = 2\frac{1}{S_{ref}} \sum_{i=1}^{N} \int_{x_i}^{x_{i+1}} 2\sin^2\alpha \, y_i dx \quad \textbf{(18)}$$

with $C_{p,l}$ the lower wing surface pressure coefficient calculated from the Newtonian Flow theory $C_{p,l} = 2\sin^2\alpha$. The upper surface of the wing span is in the shadow of the hypersonic flow so $C_{p,u} = 0.0$. Substituting the above equations of lines y_i with the corresponding x_i in Eq. (18), the estimation of the total coefficient C_N with $S_{ref} \approx 250$ m^2 gives:

$$C_N = K\sin^2\alpha \quad \rightarrow \quad C_N = 2.699092\sin^2\alpha \tag{19}$$

Lift and total drag hypersonic aerodynamic coefficients of the STS vehicle are defined in the generalized form:

$$C_L = C_N\cos\alpha = K\sin^2\alpha\cos\alpha \qquad C_D = C_{D0} + C_N\sin\alpha = C_{D0} + K\sin^3\alpha \tag{20, 21}$$

Experimental data[4] for the Space Shuttle from real flight trajectory measurements are used to determine the C_{D0} coefficient due to friction losses. In this data the maximum aerodynamic ratio $(L/D)_{max}$ is given at small angles of attack $0° \le \alpha \le 20°$. For this reason the following assumptions $\sin\alpha \approx \alpha$, $\cos\alpha \approx 1$ in Eqs. (20, 21) yield to:

$$C_L = K\alpha^2 \qquad C_D = C_{D0} + K\alpha^3 \qquad C_L/C_D = K\alpha^2/\left(C_{D0} + K\alpha^3\right) \tag{22, 23, 24}$$

At the maximum aerodynamic ratio $(L/D)_{max} = (C_L/C_D)_{max}$ (with a typical value of almost 1.9 for the most Space Shuttle hypersonic flight configurations), the C_{D0} calculation gives the following value:

$$C_{D0} = \frac{4K}{27\left[(C_L/C_D)_{max}\right]^3} \quad \rightarrow \quad C_{D0} = 0.058297 \tag{25}$$

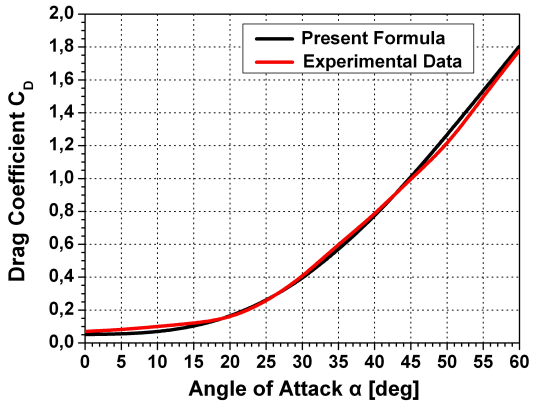

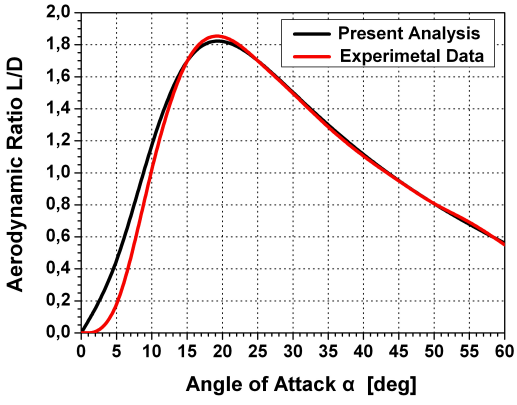

Figures 3, 4: Space Shuttle drag coefficient and aerodynamic ratio present results compared to experimental data.

Finally, the complete expressions of the aerodynamic coefficients in Eqs (20, 21) derived from the Finite Wing Span Newtonian Flow (FWSNF) model are:

$$C_L = 2.699092\sin^2\alpha\cos\alpha \qquad C_D = 0.058297 + 2.699092\sin^3\alpha \tag{26, 27}$$

The results for angles of attack from 0° to 60° using the above Eqs (26, 27) and the experimental ones are presented in Figures 3, 4. As it can be easily seen, the present analytical approach gives satisfactory accuracy in the 25°-60° angle of attack envelope. From experimental data published by NASA[4], the operational angles of attack for the Space Shuttle vehicle is 20°-60° during it's hypervelocity atmospheric re-entry mission.

3. High temperature real gas properties

As hypersonic flow encounters a vehicle, the kinetic energy associated with hypervelocity flight is converted into increasing the temperature of the air and into endothermic reactions, such as dissociation and ionization of the air near the vehicle surface. The mechanisms for this conversion include adiabatic compression and viscous energy dissipation. As a result of the change in chemical composition, the behaviour of air deviates widely from that of an ideal gas and the thermodynamic and transport properties all become functions of pressure as well as of temperature.
The aerothermodynamic analysis for entry flight in Earth's atmosphere takes into consideration the real gas properties of equilibrium air in high entry temperatures up to 15000 K as a thermo-chemically reacting gas. For the purposes of the present study, stagnation line flow has been analyzed by solving the three-equation system (continuity, momentum and energy equation) for one-dimensional friction free flow of equilibrium normal shock-wave. This method simulates the high-temperature stagnation flowfield with appropriate combinations of real gas algorithms according to Srinivasan et al.[8] where the Mollier chart of equilibrium air has been applied following the AEDC (Arnold Engineering Development Center[9]) tables as transferred in closed polynomial forms.

3.1 Stagnation convective heat flux simulation

For the hypersonic flight regime, the thermal design of the space vehicle structure and the material selection depends on the convective heating rate. Computation of the convective heat transfer[10] over the whole surface of a S/C is complicated but approximate formulas can be used for the critical estimation of the heat flux over the hottest part of the vehicle surface, which is at the stagnation point near the nose.
Accurate heat transfer predictions in the analysis of chemically reacting viscous flows for the equilibrium stagnation point boundary layer can be appreciated following the analytical correlation formula carried out by Fay and Riddell[11], taking into account that the terms containing the Lewis number is approximately 1:

$$q_S = \frac{0.763}{\left(Pr_{w,t}\right)^{0.6}}\left(\rho_{t2}\mu_{t2}\right)^{0.4}\left(\rho_{w,t}\mu_{w,t}\right)^{0.1}\left(H_{t2}-h_{w,t}\right)\sqrt{\left(\frac{du_e}{dx}\right)_{t2}} \tag{28}$$

$$\left(\frac{du_e}{dx}\right)_{t2} = \frac{1}{R_N}\sqrt{\frac{2\left(p_{t2}-p_\infty\right)}{\rho_{t2}}} \tag{29}$$

where subscript t2 denotes conditions at the stagnation point outside of the boundary layer, subscript w,t denotes properties at the wall (the inner edge of the boundary layer) and the subscript ∞ denotes the free stream conditions.
For the present study, a new modification on Fay-Riddell theory is applied based on Sutton-Graves[12] analysis. Neglecting the Lewis augmentation factor, the following simplified approximate analytical formula is proposed for calculating the convective heating to the stagnation point of a blunt axisymmetric body for gases or gas mixtures in chemical equilibrium during high-velocity entry into Earth's atmosphere by using the generalized form:

$$q_S = K_S R_N^{-0,5}\rho_\infty^{0.5}V_\infty^3 \tag{30}$$

with $$K_S = K_{S,const} K_{S,var} = 9.79714 \times 10^{-5} \left[(Z_{t2})^{0.125} (T_{t2})^{0.075} \left(1 - \frac{h_{w,t}}{H_{t2}} \right) \right] \quad \textbf{(31)}$$

V_∞ and ρ_∞ are the S/C velocity and height density free-stream values at time t for an effective nose curvature radius of R_N = 1 m for STS vehicles. The coefficient $K_{S,var}$ includes the high temperature real gas effects in the critical stagnation region. On the other hand, $K_{S,const}$ has a constant value expressed by a general relation involving the mass fractions, molecular weights and transport parameters of the base gases for the atmospheric air composition.

3.2 Simplified engineering method for wall temperature

Wall surface temperature estimations in the stagnation nose region during the descent flight phase into Earth's atmosphere is very important and critical in order to locate the appropriate thermal shielding and material-layer protection systems for the S/C body. Thus, the one-dimensional assumption energy balance for the stagnation point element[1] is considered neglecting conduction through the surfaces perpendicular to the exposed surface:

$$q_S = q_{stored,S} + q_{cond,S} + q_{rad,S} \quad \textbf{(32)}$$

The changes in the flowfield and in the wall temperature in directions tangent to the vehicle wall are relatively small. $q_{stored,S}$ and $q_{cond,S}$ are the rates at which energy is stored and conducted through the backface of the stagnation-point element, respectively, and $q_{rad,S}$ is the rate at which energy is radiated from the exposed stagnation surface. The radiative heat transfer rate follows from the Stefan-Boltzman law, with ε the surface emissivity factor (a typical value of 0.8 for STS-40[13]) and $\sigma = 5.67032 \times 10^{-8}$ W/m^{2}K^4 the Stefan-Boltzmann's constant:

$$q_{rad,S} = \varepsilon \sigma T_{w,S}^4 \quad \textbf{(33)}$$

Neglecting the energy stored in the stagnation element for steady-state calculations and incorporating the heat conducted out of the element into a adaptation factor C_{adapt} for real flight conditions (C_{adapt} = 1.06 is accurate to within 2 or 3 percent for STS vehicles[13]), the right hand side of Eq. (32) becomes

$$q_S = C_{adapt} \varepsilon \sigma T_{w,S}^4 \quad \textbf{(34)}$$

Combining Eqs (30, 31, 34), the energy balance leads to the following analytical correlation formula:

$$T_{w,S} = C_S R_N^{-0.125} \rho_\infty^{0.125} V_\infty^{0.75} \quad \textbf{(35)}$$

with $$C_S = C_{S,const} C_{S,var} = 6.718532 \left[(Z_{t2})^{0.125} (T_{t2})^{0.075} \left(1 - \frac{h_{w,t}}{H_{t2}} \right) \right]^{0.25} \quad \textbf{(36)}$$

The above-mentioned wall temperature Eq. (35) is solved numerically with an iterative Newton-Raphson procedure. For the first iteration we neglect the correction for the wall stagnation enthalpy ($h_{w,t}/H_{t2} = 0$).

4. Results and discussion

A nominal lifting entry flight of Space Shuttle STS-40 is indicated in Figure 5, entering the Earth's atmosphere with an initial elliptic velocity of 7492 m/s and flight path angle of –1.293°. The unconstrained hypersonic entry flight path of the present study compared with the corresponding optimum solution obtained by real flight data from NASA (solid blue line) indicates fluctuations, due to the important guidance variations of bank angle σ and angle of attack α during the descent flight phase[13]. Figure 6 represents the strong characteristics alterations of the entry bank angle σ versus altitude for L/D-modulation, which influence the distributions of basic aerothermodynamic re-entry flight magnitudes.

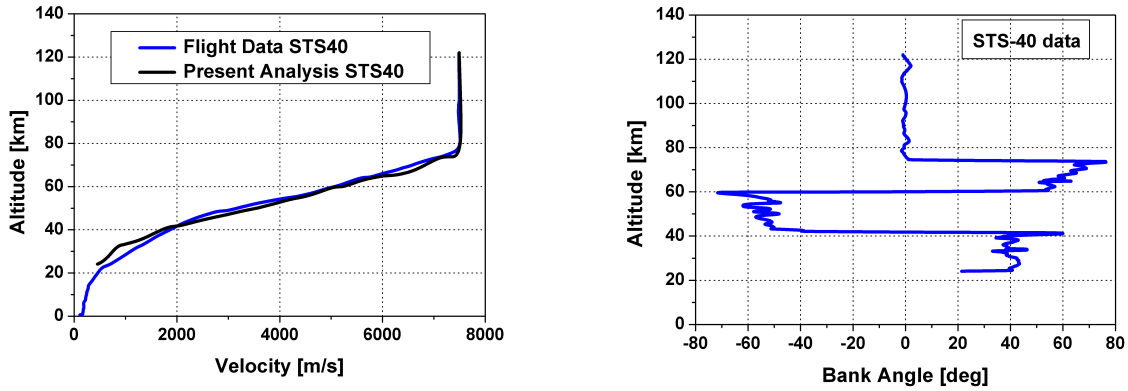

Figures 5, 6: Entry flight trajectories of STS-40 missions with the entry bank angle strong-variation history.

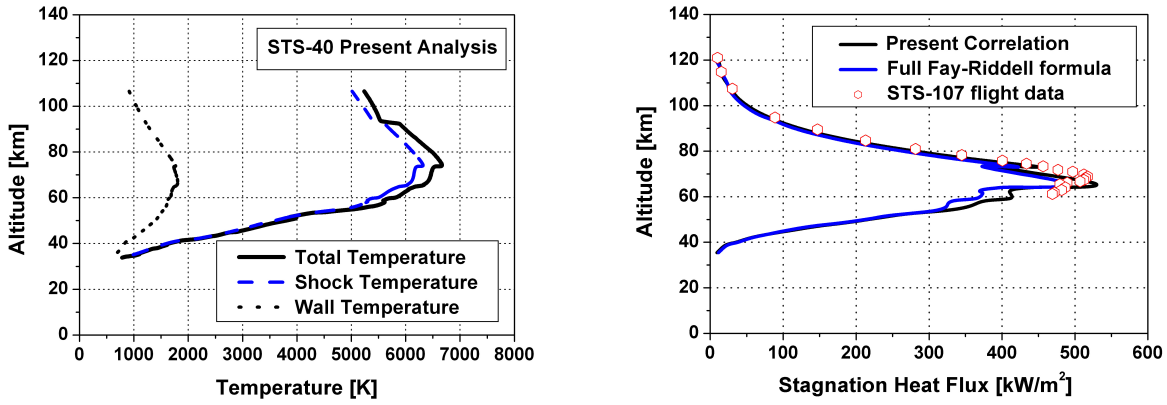

Figures 7, 8: Stagnation temperature profiles and heat flux simulations for STS-40 re-entry flight missions.

The enormous temperatures behind the bow shock wave cause the high heating loads. In the high temperature region the air ionization results to the known telecommunication entry blackout phenomenon. The critical values of the total and wall temperature altitude distributions, in the stagnation region of the lifting Space Shuttle STS-40, are presented in Figure 7. The mean wall stagnation temperature reaches a maximum value at almost 1830 K while the total temperature is approximately 6670 K appearing at about 74.5 km.

The simulation heat flux models are applied for the critical prediction of the hypersonic aerodynamic heating in the stagnation nose region for the STS-40 flight re-entry mission and are presented in Figure 8. The results of the present correlation (solid black line) including terms representing the real air equilibrium effects give a mean maximum

value of 530 kW/m^2 close to 65 km height. The computational values are in good agreement with real stagnation heat flux data from the last fatal re-entry Columbia STS-107 mission flight in 1st February 2003[14] and the full Fay-Riddell's analytical approximate correlation formula.

5. Conclusion

The 3-D dynamic equations of spacecraft flight have numerically been solved in order to predict the hypersonic nominal entry trajectory flight path of Space Shuttle vehicles into Earth's atmosphere. The applied Finite Wing Span Newtonian Flow (FWSNF) model describes very accurately the STS Orbiter aerodynamic characteristics inside the operational angle of attack "bandwidth" during its re-entry in hypersonic regime.
Parallel aerothermodynamic analysis enables the computation of equilibrium high-temperature air flow thermodynamic and transport properties on the stagnation line of the S/C. A new simplified correlation formula for equilibrium dissociated air is proposed for the hypersonic heat flux calculation at the nosecone stagnation region of the Shuttle Orbiter, based on modifications of the Fay-Riddell theory. It is used for preliminary estimation of the heat flux magnitude and for checking the results derived from complicated CFD codes.
Coupled to the suggested simulation model for the convective heat flux, the numerical solution for the temperature at the exposed wall stagnation surface was shown to give reliable estimates for STS vehicles. This demonstrates the ability of the applied coupled entry trajectory-aerothermal analysis to be further developed towards constraint conditions for current and future ballistic and lifting space mission flights in Earth (or other planetary) atmosphere.

References

[1] Panagiotopoulos, E., Margaris, D. and Papanikas, D. Aerothermodynamic analysis and real gas flow properties of spacecraft hypersonic entry flight. *AIAA Paper 2006-3250 in 9th AIAA/ASME Joint Thermophysics and Heat Transfer Conference*, California, June 2006.

[2] Papadopoulos, P. and Subrahmanyam, P. Computational investigation and simulation of the aerothermodynamics of re-entry vehicles. *AIAA Paper 2005-3206 in 13th AIAA/CIRA International Space Planes and Hypersonic Systems and Technologies Conference*, Capua, Italy, May 2005.

[3] Brauckmann, G. and Scallion W. Experimental hypersonic characteristics of the Space Shuttle Orbiter for a range of damage scenarios. *AIAA Paper 2004-2280*, September 2004.

[4] Iliff, K. and Shafer, M. Space Shuttle hypersonic aerodynamic and aerothermodynamic flight research and the comparison to ground test results. NASA/TM 4499, 1993.

[5] N. N. CAIB (Columbia Accident Investigation Board). Final Report, August 2003.

[6] Regan, F. and Anandakrishnan, S. Dynamics of atmospheric re-entry. AIAA Education Series, 1993.

[7] Sikoutris, D., Mazarakos, D., Panagiotopoulos, E., Margaris, D. and Papanikas, D. Analytical calculations of spacecrafts hypersonic aerodynamic characteristics based on experimental data. *AIAA Paper 2006-8086 in 14th AIAA/AHI International Space Planes and Hypersonic Systems and Technologies Conference*, Canberra, Australia, November 2006.

[8] Srinivasan, S., Tannehill, J. and Weilmuenster, K. Simplified curve fits for the thermodynamic properties of equilibrium air. Iowa State University, Engineering Research Institute, ISU-ERI-Ames-86401, 1986.

[9] Brahinsky, H. and Neel, C. Tables of equilibrium thermodynamic properties of air. AEDC-TR-69-89, 1969.

[10] Meese E. and Nørstrud, H. Simulation of convective heat flux and heat penetration for a spacecraft at re-entry. *Aerospace Science and Technology*, pages 185–194, 2002.

[11] Fay, G. and Riddell, F. Theory of stagnation point heat transfer in dissociated air. *Journal of aeronautical sciences,* 25:73-86, 1958.

[12]Sutton, K. and Graves. R. A general stagnation-point convective-heating equation for arbitrary gas mixtures. NASA/TR R-376, November 1971.

[13]Oakes, K., Wood, J. and Findlay, J. Final report: STS-40 descent BET products – development and results. NASA Contractor Report 189570, Flight Mechanics and Control Inc., Hampton, VA, November 1991.

[14]Nørstrud, H. and Oye, I. Re-entry simulation of the STS-107 Columbia accident. *AIAA Paper 2005-3261 in 13th AIAA/CIRA International Space Planes and Hypersonic Systems and Technologies Conference*, May 2005, Capua, Italy.

This page has been purposedly left blank